frontiers | Frontiers in Materials

TYPE Original Research
PUBLISHED 17 July 2023
DOI 10.3389/fmats.2023.1218813

OPEN ACCESS

EDITED BY
Arun Prabhu Rameshbabu,
Harvard Medical School, United States

REVIEWED BY
Manar El-Sayed Abdel-Raouf,
Egyptian Petroleum Research Institute, Egypt
Sathish Kumar Palaniappan,
King Mongkut's University of Technology North Bangkok, Thailand

*CORRESPONDENCE
D. Sarathkumar,
dsarathkumareee@gmail.com

RECEIVED 08 May 2023
ACCEPTED 30 June 2023
PUBLISHED 17 July 2023

CITATION
Sarathkumar D, Montanari GC, Sarathi R, Srinivasan M, Karthik R and Sivadasan J (2023), A new technique for recovering aged mineral oil to promote lifetime and sustainability.
Front. Mater. 10:1218813.
doi: 10.3389/fmats.2023.1218813

A new technique for recovering aged mineral oil to promote lifetime and sustainability

D. Sarathkumar[1]*, Gian Carlo Montanari[2], R. Sarathi[3], M. Srinivasan[1], R. Karthik[4] and J. Sivadasan[5]

[1]Department of Electrical and Electronics Engineering, Kongu Engineering College, Erode, India, [2]Center for Advanced Power Systems, Research Faculty III, Florida State University, Tallahassee, FL, United States, [3]Department of Electrical Engineering, Indian Institute of Technology Madras, Chennai, India, [4]Department of Electrical and Electronics Engineering, Valliammai Engineering College, Chennai, India, [5]Department of Electronics and Communication Engineering, PSR Engineering College, Sivakasi, Tamil Nadu, India

Using mineral oil (MO) derived from petroleum, e.g., transformer insulation, raises environmental risk and affects sustainability. Due to its affordability and easy availability, MO will ineluctably be preferred over other biodegradable oils. Therefore, tools must be developed to recover aged MO, extend the life cycle, and increase its sustainability. The work presented here is aimed at the investigation of the electrical insulation properties of thermally-aged recovered-aged mineral oil (RAMO), as well as of aged cellulose pressboard impregnated by fresh mineral oil (FMO), aged mineral oil (AMO), and RAMO. The AMO is recovered using the combined adsorbents, A* and B*, which are Chitosan-activated Bentonite (CTN-aB) and Polyaniline coated Kapok Fibre (PANI-c-KPF) mix. According to FTIR, the recovered oil, RAMO, displays less C=C double bonds and carbonyl vibrations at 140°C, indicating lower oil ageing compared to AMO. The distribution of the crystalline and amorphous peaks is uniform for aged oil-impregnated pressboard (PB) with FMO and RAMO. Overall, it has been discovered that PB is impregnated with RAMO, resulting in an extended lifetime for the solid insulation. As a result, the increase in emissions slows down, and global sustainability targets are met.

KEYWORDS

aged mineral oil, combined adsorbents, pressboard insulation, thermal ageing, reclamation

1 Introduction

Sustainable transformer operation is achieved by balancing the potential environmental risk, primarily due to mineral oil and impregnated paper used as insulation, with low-cost solutions for extending insulation life and reducing environmental impact. Transformer reliability depends on insulation system design and the ageing performance of insulating materials (Raj and Murugesan, 2022). Cellulose paper and pressboard provide electrical insulation and mechanical supports (Raymon et al., 2015). Transformer oil serves as an insulator and a coolant. For years, fresh mineral oil (FMO) was chosen for its better dielectric strength. However, intrinsic and extrinsic ageing effects of thermal and electrical stresses, plus external contamination, drive FMO to transform into aged mineral oil (AMO). Reduced electrothermal properties of AMO

can cause transformer failure, with the risk of explosion, oil leakage and, in general, environmental damage. On the other hand, replacing AMO planned to avoid failures canalso be environmentally problematic if not carried out properly (AMO can disperse toxic dioxins and furans into the environment) (Raymon et al., 2015) (Sangeetha et al., 2019). In summary, these oils must either be recycled into a potential dielectric or transformed into the trash by disposal. Natural fibre-based biodegradable composite reportedly shows a lot of environmental protection against the recycling and disposal of materials (Mohan et al., 2023). In both scenarios, the need for investment in oils and reclamation costs increase, but the latter causes additional sufferance to the ecosystem due to the larger consumption of FMO. Hence, a significant capital shift from oils to reclamation would be necessary to achieve sustainability targets.

The presence of contamination in oil (which can increase with ageing under operation) and metal particles in oil or paper, delamination, and gas bubbles in the oil can cause accelerated extrinsic insulation ageing (Safiddine et al., 2017). Polar molecules, including a group of carboxylic acids, will develop in paper due to electrothermal stress (Lelekakis et al., 2014; Amizhtan et al., 2020), damaging cellulose chain structure. Further degradation reactions are induced by moisture, ultimately fracturing the cellulosic structures. Acids and sludges are produced when oil oxidises, which causes oil to degrade. Pressboard absorbs low molecular weight acids, facilitating the protonation that damages the pressboard matrix (Amizhtan et al., 2020; Liao et al., 2008).

Longitudinal cellulose molecules composed of α - D units split apart at temperatures over their normal operating range. Electrothermal ageing also causes leftovers of the furan as a side product (Karthik et al., 2013). The oxygen content of FMO is frequently low, and it may form carboxylic groups when exposed to high temperatures and water molecules. When FMO-AMO lack inhibitors, such as 2,6-di-tertiary-butyl-phenol (DBP) or 2,6-di-tertiary-butyl-para-cresol (DBPC), they are not capable of neutralising oxygen species anymore (Safiddine et al., 2017; Raymon et al., 2022), thus oil age faster. Additionally, FMO exhibits low dielectric breakdown voltage when few water molecules are present. AMO integrates the protonation with the pressboard, making it highly reactive under normal and extreme temperature ranges (Sarathkumar et al., 2022). Removal of contaminants, ageing byproducts, polar compounds, water, acids, metals, and sludges is required to restore AMO (Vasa et al., 2017). Several AMO reclamation approaches were presented in the literature, aiming to restore AMO dielectric performance in line with those of FMO. Indeed, if effective, RAMO would be an essential tool in reducing the exploitation of petroleum resources.

This paper proposes using innovative natural resource-based adsorbents coupled to bring the AMO back to acceptable electrical insulating levels. By doing this, the amount of AMO that is burned and dumped waste is significantly decreased, positively impacting the environment, safety and health (e.g., carcinogenic consequences). According to literature, attempts made to limit the use of FMO in transformer applications utilising natural esters, synthetic oil, and their mix with FMO have had some success since it was proven that pressboards age at a lower rate than those impregnated by FMO. Upon utilising the mixed adsorbents strategy introduced here, performance would improve since the new method effectively eliminates polar and non-polar pollutants. The validity of the proposed approach is proved by accelerated thermal ageing of RAMO and RAMO-impregnated pressboard under controlled conditions, measuring various electrical, physical, chemical and mechanical properties. It is conceivable to achieve the sustainable target using an adsorbent approach. However, doing so would necessitate more efforts to decrease pollutants in other ways, making it more challenging to meet high environmental objectives.

The utilisation of biodegradable or green adsorbents provides the exact solution to the above problem. (Sathish Kumar et al., 2023). Hence adsorbent plays a crucial role in removing impurities from the RAMO, thereby regenerating its dielectric functions like the FMO. The superior adsorbent properties of chitosan, activated bentonite, and polyaniline-coated Kapok fibre are richly utilised. Both chitosan and bentonite have excellent adsorption ability when fused, giving out thermal stability. These compounds are naturally occurring and readily biodegradable.

On the other hand, polyaniline is an organic polymer with good environmental stability, which is coated with kapok fibre, a naturally occurring fibre, to remove waxy cutin. These PANI fibres provide excellent mechanical properties, as well as adequate chemical resistance and thermal stability, and their ability to absorb and remove heavy metals is greatly improved by PANI-c-Kapok fibres. These superior properties of the materials are richly utilised in this research to remove impurities in AMO and, at the same time, regenerate its dielectric properties much more suitable for transformer applications.

Sections 2 explains the procedures used to produce adsorbents, recover AMO and prepare pressboard samples for ageing. Measurements of the different mechanical, electrical, chemical, and physical properties of the pressboard both before and after ageing are covered in Section 3. The investigation of oil sample properties before and after ageing is dealt with in Section 4. Discussion, aiming at demonstrating the adsorbent capability to recover the aged oil, hence, to slow down impregnated PB ageing or to increase PB lifetime, is developed in Section 5.

2 Experimental procedures

2.1 Materials

The materials used in the investigation are given a code to simplify the understanding of the combination of adsorbents, and the composition of materials is presented in Table 1.

Chitosan and activated Bentonite were compounded together to obtain a homogenous blend. The Chitosan compound with the following characteristics was bought from Bangalore Fine Chem in Bangalore, India: density 0.25 g/cc, degree of deacetylation >88%, moisture 6%–8%, viscosity 50–80 CPS, and ash content 0.5%. The sodium-activated bentonite was bought from Ecotika in Gujarat, India, and has the following characteristics: the maximum crystalline size of 101 nm, density of 2–3 g/cm^3, and molecular weight of 422.29 g/mol after activation with 4M sodium hydroxide. CTN is a polymer containing anionic amino groups and cationic hydroxyl groups, which has a potent electrostatic attraction that may extract non-polar impurities from the oil (Yashvi et al., 2021). It draws pollutants due to its hydrophilic quality, which also causes it to expand like a spongy gel. However, at higher temperatures,

TABLE 1 Materials code and composition.

Adsorbent	Chemical formula	Acronym	Composition used (g)	Code
Chitosan	$C_{18}H_{35}N_3O_{13}$	CTN	5	A*
Activated Bentonite	$Al_2H_2Na_2O_{13}Si_4$	aB		
Polyaniline	C_6H_5N	PANI	5	B*
Kapok fibre	-	KPF		

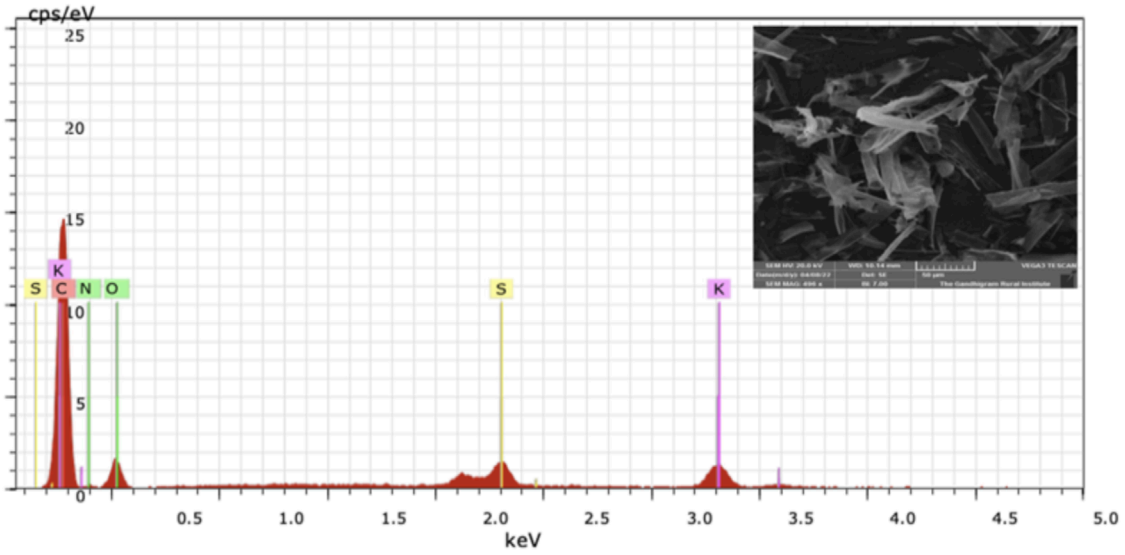

FIGURE 1
EDX shows the adsorbent A* morphology and elemental mapping.

CTN becomes brittle and mechanically unstable. Two tetrahedral layers can be sandwiched together to form an aB structure (i.e., octahedral sheets with exchangeable cations) that has expanding shape, allowing aB to intercalate smaller molecules while absorbing polar groups (Raymon et al., 2015) (Veerakumar et al., 2021).

The Polyaniline-coated Kapok fibre adsorption capability is also utilised in the following investigation. The kapok fibre coating with polyaniline was prepared at the laboratory. The industrial polymer PANI, which is affordable and well-known, is the one most frequently utilised as a precursor in the manufacturing of carbon fibres. (Dominic et al., 2022). Polyaniline has a molecular mass of 91.11 g/mol and is coated with the Kapok fibre. Kapol fibre, a natural fibre with a high surface area to volume ratio that is readily available, was chosen. Its main components are wax, lignin, and cellulose.

2.2 Preparation of adsorbent A*

The properties of aB and CTN are homogenised by a method known as mechanochemical synthesis. The morphology and the elemental Energy Dispersive X-ray Analysis (EDX) of adsorbent A* are shown in Figure 1. When polar and non-polar pollutants are adsorbed on the homogenised A* = aB-CTN, their expanding nature results in a monotonous adsorption site.

2.3 Preparation of adsorbent B*

PANI molecules include an abundance of reactive nitrogen-based groups, such as amino and amine groups, which are advantageous for binding sites for sorption stimuli that can be applied to Kapol fibre to perform removal procedures. These shoes are oxidised and in the pernigraniline stage. The huge hollow hole in the Kapok fibre may be useful for creating adsorbent polymers. However, the hydrophobic fibre properties are one of its drawbacks because of its waxy cutin. Therefore, a hydrophilic substrate—such as modified Kapok fibres rendered hydrophilic by polymerisation with several amine groups—is necessary for particle embedding in an aqueous medium (Rontgen et al., 2020). By this approach, PANI micro and nanofibres are now being employed to create adsorptive membranes (Dominic et al., 2022) in addition to serving as efficient adsorbents for the removal of toxins and pollution-causing chemicals from water and wastewater effluents. The morphology and the elemental Energy Dispersive X-ray Analysis (EDX) of adsorbent B* are shown in Figure 2.

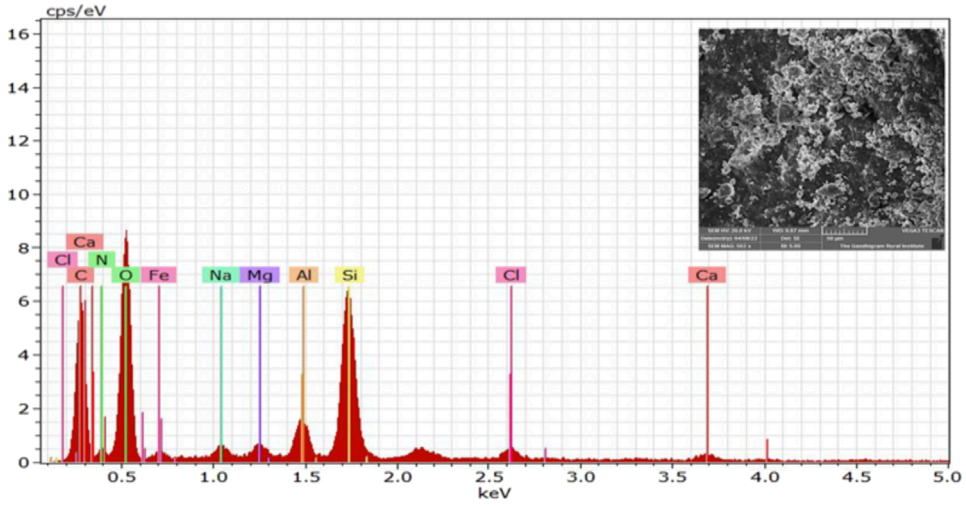

FIGURE 2
The adsorbent B* morphology and elemental mapping.

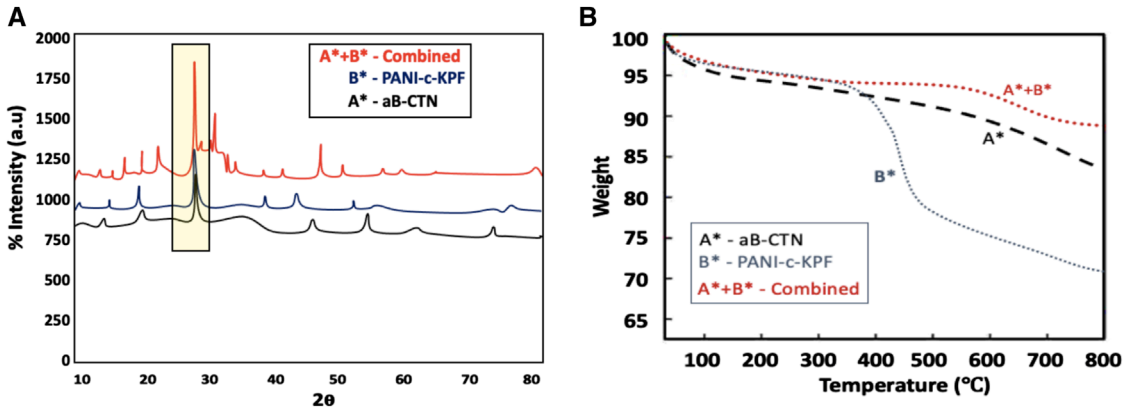

FIGURE 3
A*+B*, A*, and B* characteristics as determined from **(A)** changes in the material's crystallography using XRD and **(B)** changes in the material weight using TGA.

2.4 Preparation of adsorbent A*B*

A* B* is obtained by compounding them in a ball mill using mechanochemical synthesis. A weight ratio of 5 g:5 g is taken, and the mixture is first crushed and ground using steel ball charges. The process is continued on a micro-scale for three hours at 75 rpm, reducing the mixture to a fine powder. The materials examined were crushed using the rotatory ball mill until a powder form is obtained. The figures show that the mix is unaffected by the aB crystalline structure and that A*+B* have lower thermal degradation than A* and B* separated.

The structure of the absorbents, A*, B*, and A*B*, are investigated using X-ray diffraction (XRD), depicted in Figure 3A. The XRD analysis uses Cu-Kα radiation with a wavelength of 1.5418 Å, the average of Ka1 and Ka2 and scan speeds ranging from 3 min^{-1}. The temperature of the measurement was set to 0°–80°C. The analysis uses a step size of 0.05 and high voltage and a current of 30 kV and 20 mA for accuracy. In the reflection mode, an XRD pattern's range was between 10 and 80. In contrast, the thermal degradation is inferred through thermogravimetric analysis (TGA), Figure 3B. Using the thermal analyser, the sample was heated up to 800°C at a scanning temperature of 5 °C/min in a nitrogen environment, and the adsorbents' thermal properties were examined. The crucible was built of alumina, and the inert gas flow was kept at 150 mL/min constant.

2.5 Preparation of the RAMO

The AMO used as a base fluid in the experiments underwent the treatment process depicted in Figure 4. The combined adsorbents were weighed at 1.76 and 1.28 g per 250 mL, heated to 78.9°C, and

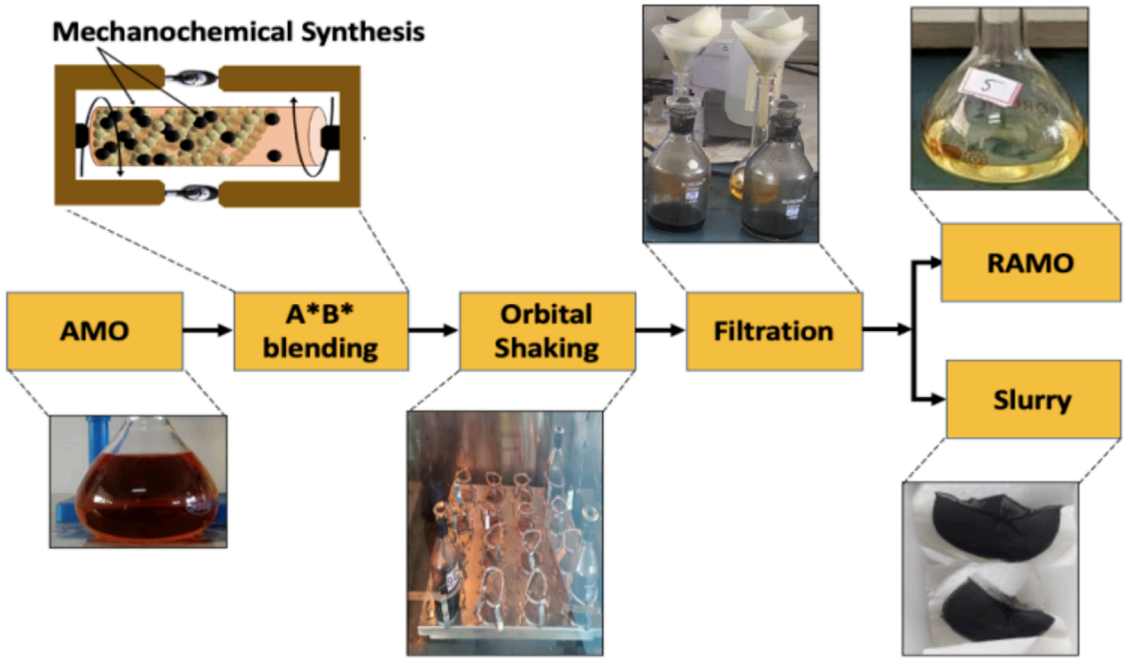

FIGURE 4
The treatment process of the AMO.

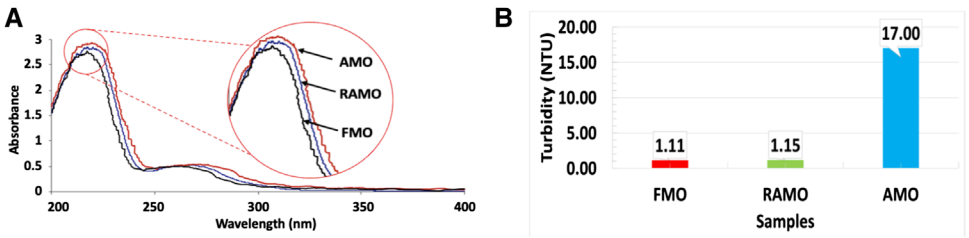

FIGURE 5
Absorbance and Turbidity of oil samples, **(A)** UV-VIS spectrum of AMO, FMO, and RAM, **(B)** Comparison of the turbidity of oil samples before and after adsorbent treatment.

then agitated for three hours in an orbital shaker. A Whatman filter paper was used to filter the mixture after pouring it into a funnel (Figure 4).

The ultraviolet (UV) responses were recorded and shown in Figure 5A, indicating several electronic transitions with different amounts of energy absorption. The peak at 380 nm indicates a low energy transition with minimal energy absorption.

The presence of byproducts in AMO is connected to the conjugated C=O linkages. AMO is associated with more considerable energy because of the high concentration of byproducts smaller than 300 nm. Turbidity measurements were carried out according to ASTM D6181-03 (ASTM, 2003) and D3487-09 (ASTM, 2009). Results are shown in Figure 5B. The turbidity of the AMO is 17 NTU, while that of RAMO is 1.5 NTU, which is very close to that of FMO, i.e. 1.11 NTU.

2.6 Preparation of the pressboard

The oil was dried for five hours at 100°C, to remove the moisture, and degassed. A high-density (1.2 g/cm^3) "KPC" grade pressboard, with a surface area of 4 cm^2 and 1.5 mm thick (from Padmavahini Transformers Pvt. Ltd., Coimbatore, TN, India) was used for the research. Pressboard impregnation was prepared according to International Electrotechnical Commission (IEC) 60,641–2 (Karthik et al., 2013). The pressboard material was dried for 24 h at 110°C in a hot air oven to remove any moisture content. The Oil Impregnated Pressboard (OIPB) was prepared by piling a dry pressboard up to a height of 15 mm in an oil container with 30 mm of oil, ventilated at 80°C for 8 h. After this procedure, summarized in Figure 6, the dried pressboard was wrapped with a copper sheet 0.5 mm thick (to simulate real operation), and placed

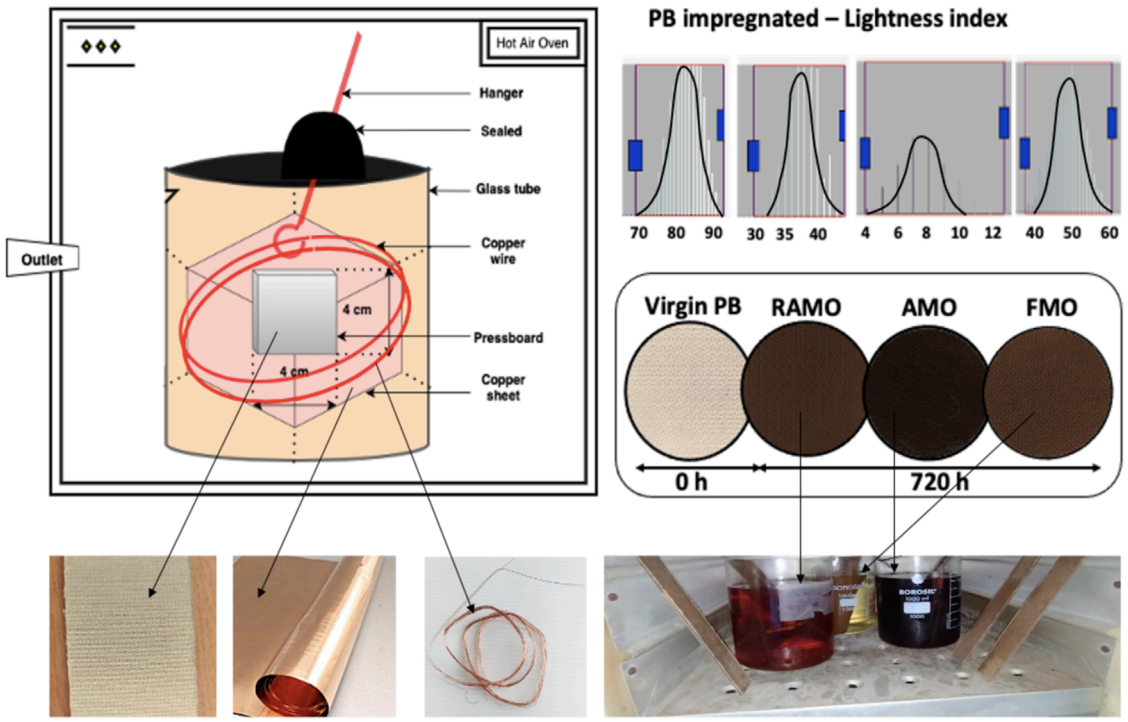

FIGURE 6
Ageing chamber with pressboard maintained for 720 h at 140°C, and recording of the colour of each pressboard sample before and after ageing (virgin means unaged).

in a reaction tank with 1 L of oil (Amizhtan et al., 2020), where it was submerged at 90 °C for further 24 h to achieve impregnation. The weight proportion of the vessel pressboard, copper, and oil was 10:1:1. A temperature-controlled oven was used to conduct the thermal ageing experiment, lasting for 30 days, or 720 h, at 140°C.

3 Results and discussion for PB samples

3.1 Measurement of tensile strength

Since tensile strength measurements reveal details about the sample stiffness and elastic limit, estimating the paper shear strength is one of the most important markers (Carmela et al., 2021). As in-plane uniaxial testing at 45° to the machine direction yields a biaxial stress state similar to a pure shear condition, some sources advise utilising this stress state to evaluate the shear properties of paper. Paper materials with the same composition and density as those mentioned above were considered as an alternative to 90° testing. A 35° angle to the machine direction was shown to effectively derive the shear stress component while limiting the impact of other stress components (Yoshihara et al., 2014). The pressboard utilised in this study was oriented at a 35-degree angle in accordance with American Society for Testing and Materials (ASTM) D638 (ASTM, 2014) requirements, and the experimental setup is shown in Figure 7.

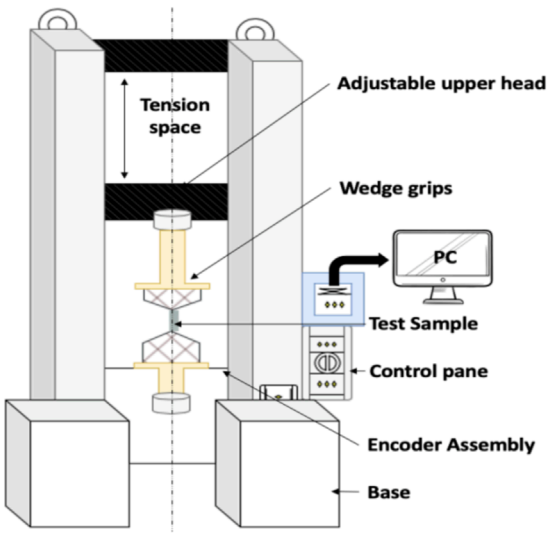

FIGURE 7
Experimental setup–Universal Testing Machine interfaced to PC.

The tensile stress-strain relationship of the OIPB samples in comparison to unaged PB is displayed in Figure 8 when impregnated with AMO, FMO and RAMO. Table 2 reports the elongation at break and percent elongation values of the various PB-impregnated materials. It also shows that virgin PB has the largest elongation

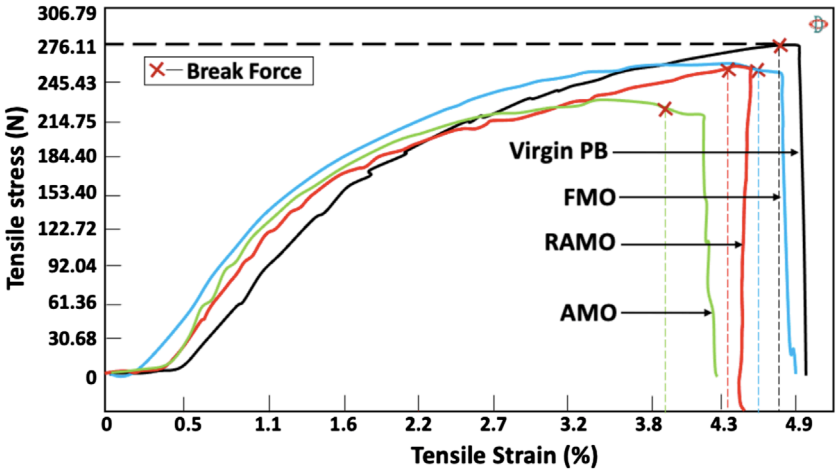

FIGURE 8
The stress-strain curve comparison between unaged (virgin) PB and OIPB samples, using FMO, RAMO and AMO.

TABLE 2 PB material's elongation response after ageing.

PB impregnation	Break elongation (mm)	% elongation
Virgin PB—0 h	4.8	9.6
FMO—720 h	4.6	9.3
RAMO—720 h	4.3	9.0
AMO—720 h	3.2	6.8

at break and percent tensile strain of all the tested PB samples (Figure 8).

Ageing is likely to cause the interaction of water molecules and the hydroxyl groups in the cellulose chain, with the consequence of the breakdown of polymers hydrogen bonds, and scission of the lengthy cellulose chains, which leads to a lower degree of polymerisation and decrease of their mechanical strength (Amizhtan et al., 2020; Coulibaly et al., 2013). After ageing, impregnated pressboards exhibit a decrease in percent tensile strength and elongation at break, respectively, in the following rank: unaged PB (4.78%:4.8 mm), FMO (4.35%: 4.64 mm), RAMO (4.32%: 4.33 mm), and AMO (3.9%: 3.2 mm). Hence, the PB impregnated with RAMO keeps a larger elastic strain than the AMO, as seen by the ratio between % tensile strain and elongation at break.

3.2 Thermogravimetric (TGA) analysis

The experimental setup of TGA is shown in Figure 9. When the substance was exposed to exothermic heat, the material decomposes chemically. PB and OIPB samples was heated up to 600° with temperature rise rate of 5°–50 °C/min (dynamic TGA measurement), recording weight variations, see Figure 10A. The percentage of the sample mass change is provided through Derivative Thermogravimetry (DTG), Figure 10B. Weight loss, due to bulk degradation (molecular breakdown), is evident, especially in AMO specimens, see Figures 10A, B, the latter also highlighting decomposition spots.

Phase transition, absorption, desorption, and thermal decomposition are a few examples of the physical characteristics that change because of the molecular decomposition. Interestingly, it appears that the maximum decomposition rate of the RAMO-impregnated PB is lower than that of AMO-PB, see Figure 11. Also, the first decomposition peaks are quite similar regarding magnitude and temperature for OIPB with RAMO and FMO. The former, however, has two peaks and the first occurs at about 180°C (while that of FMO is 200°C). Let us note that the first peaks for FMO and RAMO indicates that the PB is undergoing a gradual degradation already from first decomposition states. AMO has a weak first peak, which may suggest that the ageing process can start at lower temperatures and involves less energy due to lower degree of polymerization.

3.3 Evaluation of PB pattern using XRD

The X-RAY diffraction method allows the degree of crystallinity to be evaluated. (French, A.D., 2014). Pressboard is made of amorphous lignin and crystalline cellulose. The X-ray diffraction test was performed by the PRO Panalytical model "X" (Karthik et al., 2013) and the XRD pattern of different PB samples is given in Figure 11. Crystals distort the wave nature to produce a characteristic pattern of peak "reflective surfaces" at different angles and of varying intensities. As it scans through the sample, the X-ray detector notices the size and location of these peaks. The analysis of the material relative crystallinity makes use of the diffraction intensity of amorphous region (I_{am}) and the diffraction intensity of crystalline region (I_{200}). The relative crystallinity (CrI) may be computed from Eq. 1 (French, 2014).

$$CrI = [(I_{200} - I_{am})/I_{200}] * 100\% \quad (1)$$

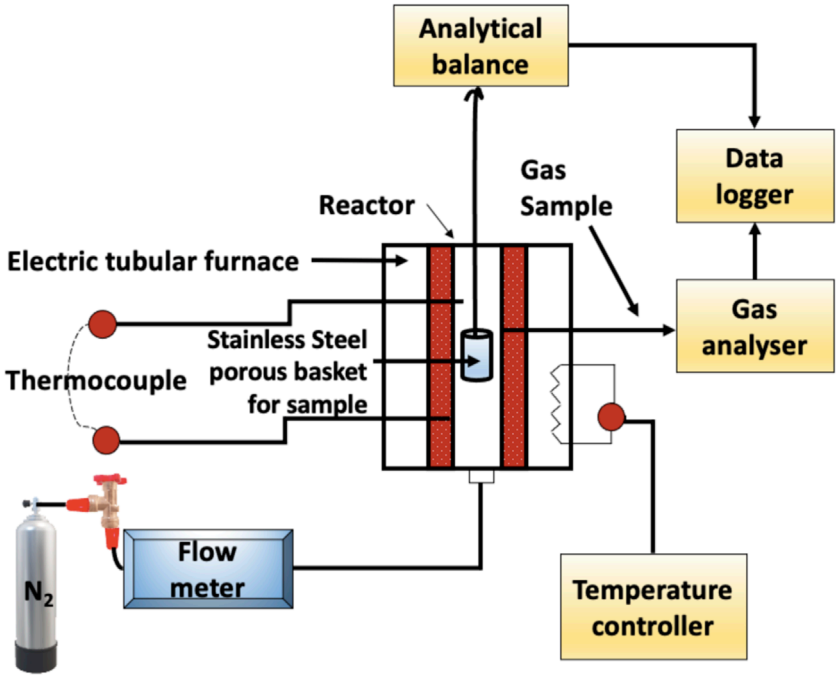

FIGURE 9
Experimental setup–TGA.

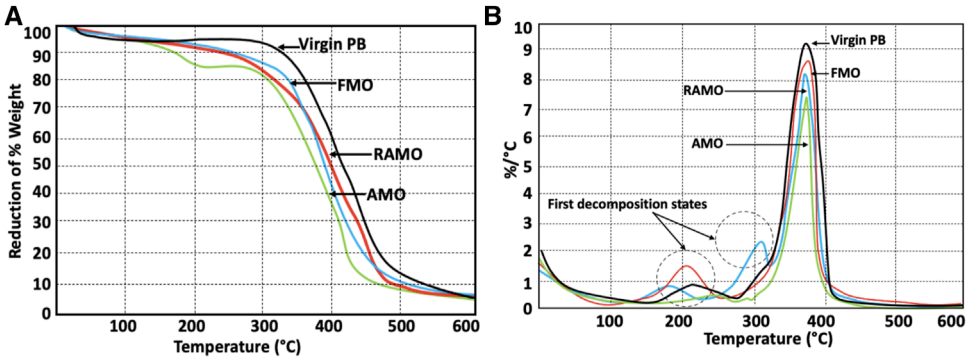

FIGURE 10
Decomposition of PB, **(A)** Temperature vs. % weight reduction of Virgin PB materials and OIPB, from TGA, **(B)** Comparison of virgin PB sample with OIPB sample using derivative thermogravimetry (DTG).

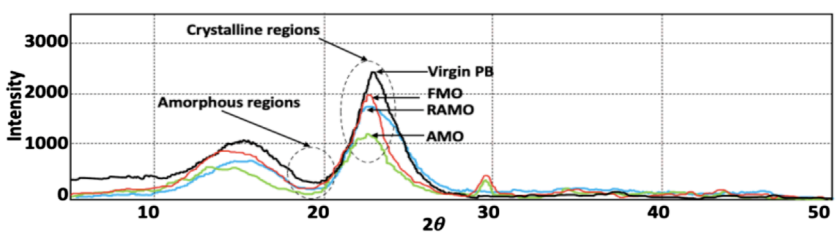

FIGURE 11
Comparison of XRD patterns of virgin PB and OIPB samples.

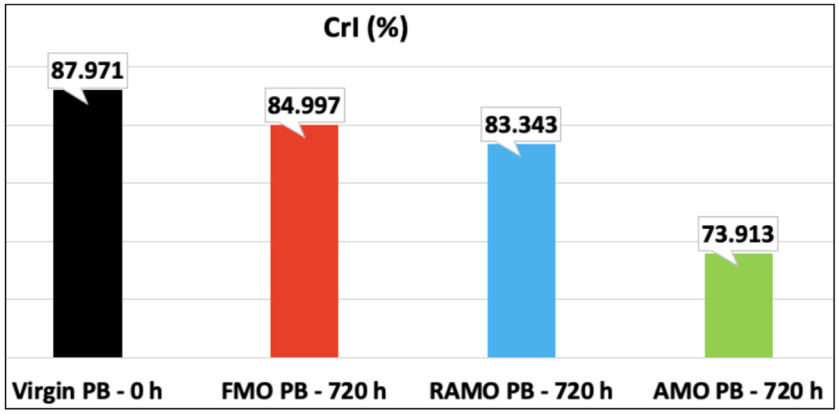

FIGURE 12
Comparison of relative crystallinity of virgin PB and OIPB samples.

In addition to the relative crystallinity, another measure that might represent changes in the polymer materials is the crystallite size (Neettiyath et al., 2021; Segal et al., 1959). Pressboard is amorphous and crystalline XRD patterns are depicted in Figure 12. Peaks in the PB that are aged using AMO become less intense than with RAMO and FMO, due to weakening due to broken cellulose. The peaks of the PB samples after treatment with RAMO and FMO are very close, indicating that the PB has retained its cellulose. Typical relative crystallinity values of the tested PB samples are compared in Figure 12, showing that PB impregnated by AMO have the largest drop due to thermal ageing. In contrast, RAMO and FMO have close performance.

The fact that OIPB treated with RAMO has peak and relative crystallinity that are closer to those of FMO highlights that the combined adsorbents effectively remove polar and non-polar impurities (Sarathkumar et al., 2022). Due to the cellulose chain scissions, the reduction of crystallinity may also impact on the size of the crystals. Similar findings were found in research that revealed a decrease in crystallinity and the size of the crystals of pressboard aged in MO and concluded that this was due to the D-glucopyranose unit connection breaking (French, 2014).

3.4 Scanning electron microscope (SEM) observations

The HITACHI model S-3000H with a magnification of up to ×500 and x250 was used for the SEM experiments. Observations are summarised in Figure 15. Pressboard is typically made of cellulose and lignin fibres that have been tightly knitted together (Figure 13D) (Amizhtan, 2020). Figure 13A emphasises that cellulose fibres are not organised in the right order. The side walls of the cellulose fibre structure have perforations. As indicated by Figure 13A, the ageing phenomenon affects the material's structural integrity by weakening and detaching the intermolecular fibres from the polymer chain.

In general, the PB impregnated with AMO has more broken fibres when compared with PB impregnated with RAMO (Figure 13B) and FMO (Figure 13C), which suggests smaller deterioration. The pressboard cellulose structure is broken down into shorter chains, and the production of hydroxyl compounds may reduce the pressboard tensile strength and relative crystallinity, see Figures 8, 12, as well as its polymerisation level.

3.5 Breakdown voltage (BV) measurements

IEC 60243 (IEC, 2013) standard was used to test the six PB samples for AC breakdown voltage at 1 kV/s increasing voltage rate. The electrode spacing in oil was 3 mm, and 6 mm apart, multiples of 2, and 4 of pressboard 1.5 mm thickness (Dawei et al., 2020). Hemispherical electrodes are used. The test oils are poured into the gap between the surfaces of the pressboard and the electrodes, and the pressboard sample is positioned in the middle between the electrodes. The results are displayed in Table 3.

The OIPB with RAMO (OIPB-RAMO) at 0 h and 720 h typically exhibits a much larger AC breakdown voltage than the OIPB with AMO, which can be due to the free path length (for aged specimens) and polar and non-polar impurities. The OIPB-FMO has the best performance, as expected, but the rate of BV decreases with ageing is similar to OIPB-FAMO. On the other hand, enhanced PB dielectric strength and dielectric dissipation factor are seen in the OIPB sample aged in RAMO, compared to AMO. Due to increased insulation caused by its low dielectric dissipation factor, as shown in Table 4, the breakdown voltage of PB impregnated in RAMO has percent drop similar to FMO.

4 Results and discussion for oil samples

4.1 Evaluation of oil samples using COLOUR

Colour indices are used to quantify the removal of polar and non-polar components from the tested AMO (indices were

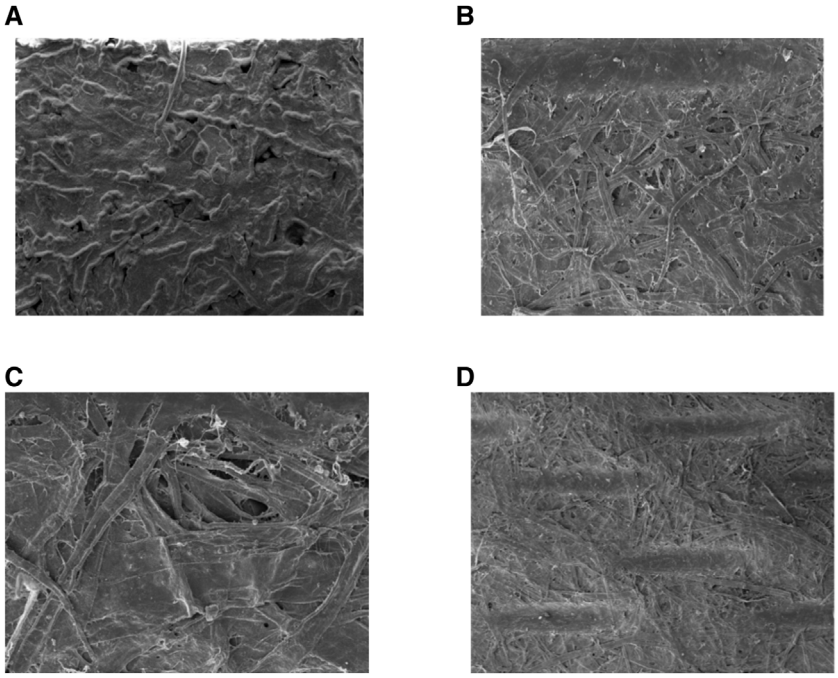

FIGURE 13
Morphology of PB samples after ageing for 720 h, **(A)** AMO, **(B)** RAMO, **(C)** FMO, and **(D)** Virgin PB.

obtained using the CR-200 Chroma Meter (Minolta)). In accordance with the International Commission on Lighting, the parameters L*, a*, and b* were measured using a light box with fluorescent D50 illumination, a Motrox Meteor image capture card, and an integrated Sony camera (CIE) (CIE, 1995). Here, the removal of sludge by A* and B* is shown by the lightness index L*, while the removal of metal ions and organic compounds is indicated by the chromaticity of a*. As an alternative, the decrease in a* shows that electrochromism occurs at active redox sites brought on by electron loss. The colour chromaticity is shown in Figure 14A. b* stands for the chromaticity of blue and yellow. The increase of b* indicates that water has been taken from RAMO under investigation. An inverted or stimulated colour change is the consequence which is shown in Figure 14B.

The oil samples' mean dielectric breakdown voltage and dissipation factor under investigation were estimated to have new levels that satisfy IEC standards 60,156 and 60,247 (IEC, 2004; IEC, 2023). Table 3 compares the results, showing that improvement of dielectric breakdown voltage and dielectric dissipation factor of the test oil samples treated and aged with and without the A*+B* is achieved.

4.2 Evaluation of oil samples using fourier transform infrared (FTIR)

A Perkin Elmer PE 1000i spectrometer with a microscope and a mercury-cadmium-telluride detector were employed for FTIR

TABLE 3 Electrical properties of the Test PB before and after ageing with the test oils.

Sample	AC dielectric breakdown voltage (kV/mm)	
	Electrode spacing = 3 mm	Electrode spacing = 6 mm
FMO—0 h	68.6	76.2
FMO -720 h	64.4	72.8
AMO—0 h	45.2	54.0
AMO—720 h	41.0	44.0
RAMO—0 h	59.0	70.0
RAMO—720 h	53.8	67.6

TABLE 4 Electrical properties of the Test oils before and after treatment with A*+B*, and before and after ageing.

Sample	Breakdown voltage (kV/2.5 mm)	Dissipation factor at 90°C (kV)
FMO—0 h	48	0.0018
FMO -720 h	46	0.0019
AMO—0 h	21	0.2112
AMO—720 h	8	0.3730
RAMO—0 h	44.2	0.0020
RAMO—720 h	41.6	0.0025

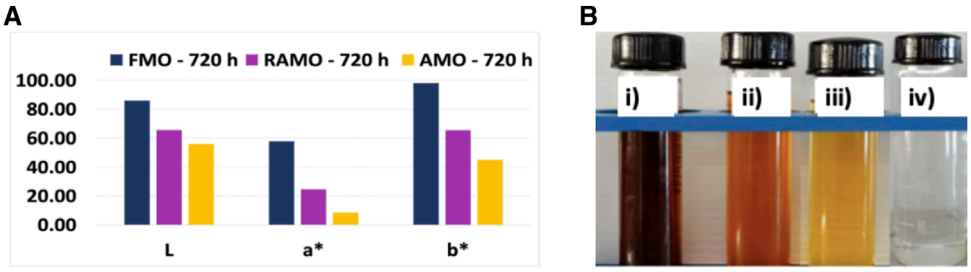

FIGURE 14
Colour Chromaticity, **(A)** Chromaticity changes in the PB-impregnated oil samples after ageing for 720 h, **(B)** Colour changes in the PB-impregnated oil samples after ageing for 720 h: i) AMO, ii) RAMO, iii) FMO, in comparison with the iv) FMO without ageing (Unaged).

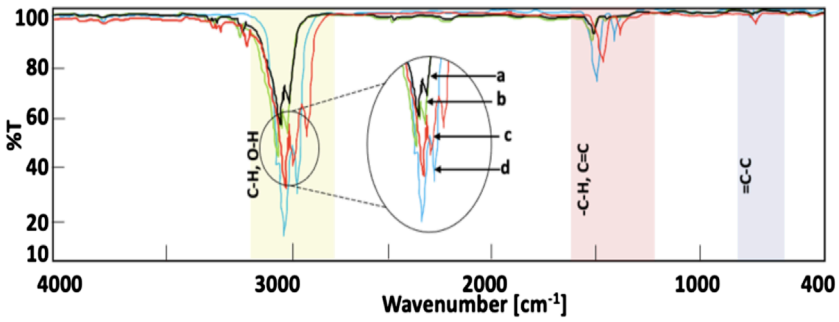

FIGURE 15
FTIR spectrum of oil samples **(A)** RAMO—0 h, **(B)** RAMO—720 h, **(C)** AMO—0 h, **(D)** AMO—720 h.

measurements. A diamond anvil cell was used to obtain spectra with a scanning speed of 2 mm s^{-1}, a gain of 8, a 45-degree incidence angle, a resolution of 4 cm^{-1}, and considerable Cosine apodisation. The spectra were obtained for the range from 4,000 to 400 cm^{-1}. The FTIR results for the oil samples are displayed in Figure 15.

The spectra revealed the presence of three functional groups in the ranges of 650–800 cm^{-1}, 1340 to 1600 cm^{-1}, and 2820 to 2980 cm^{-1}. The peak (of limited intensity) in the range of 2820–2980 cm^{-1} can be associated with acids and alkanes, while the larger peak between 1340 and 1600 cm^{-1} is related to aromatic functional groups. The absorption of the = C-C band causes a small oscillation at 742 cm^{-1}. The maximum carbonyl absorption occurs at 1351 cm^{-1}.

Additional evidence of the presence of double bonds may be found in the bands at 3107 cm^{-1} and 3119 cm^{-1}, which are generated by the stretching vibrations of the C-H moieties at the C=C band. The treated AMO spectrum reveals that the carbonyl vibration is somewhat shifted in the aged material, moving from 1534.11 to 1585.17 cm^{-1}. After A*+B* treatment, the strongest signals in the RAMO spectrum, caused by vibrations at 1512.61 and 1549.28 cm^{-1}, exhibit notable reduction compared to AMO. This indicates that A*+B* can bind both polar and non-polar molecules, thus improving oil dielectric properties (Sarathkumar et al., 2022).

5 Conclusion

The aged mineral oil was successfully recovered in this study using a combination of adsorbents, A* and B*. It is shown that the Reclaimed Mineral Oil electrical characteristics can be restored close to those of FMO. The electrical, mechanical, and thermal characteristics of the PB samples aged in RAMO are superior to those impregnated by FMO. Overall, this study yielded several conclusions, including the following.

1. Combining A* and B* enhances the compound's ability to adsorb ageing by-products.
2. The turbidity of the recovered oil Ultraviolet radiation proves that most byproducts have been eliminated. Colour indices further demonstrate the removal of polar and non-polar contaminants.
3. The mechanical strength of the PB (i.e., elongation at break and % elongation) confirms that the ageing of OIPB with RAMO has a limited impact on the polymer hydrogen bonds and scission of the long cellulose chains, as for FMO.
4. TGA indicates that RAMO molecular breakdown rate is comparable to FMO, which relates to slower degradation than AMO.
5. XRD shows that relative crystallinity for OIPB with RAMO recovers to a value near FMO.

6. According to SEM, OIPB aged in RAMO and FMO have comparable patterns, highlighting significant intermolecular fibre structural integrity.
7. The breakdown voltage values of oil and OIPB samples before and after ageing are further evidence of the adsorbent ability to recover electrical insulation performance.
8. The oil dissipation factor indicates that RAMO effectively eliminates polar groups due to ageing.

All these points support the effectiveness of the A*+B* reclamation strength. This suggests that the reuse of the aged oils in transformers can be implemented without compromising the dielectric properties of the PB. In this way, the importation and adulteration of oils and risks associated with incineration will decrease by implementing the suggested reclamation technique, which could become an environmental-sustainable, win-win, cost-effective solution.

Data availability statement

The original contributions presented in the study are included in the article/Supplementary material, further inquiries can be directed to the corresponding author.

Author contributions

Conceptualisation, DS and MS; methodology, DS and MS; data curation, DS, MS, and JS; investigation, writing-original draft, DS, MS, and RK; writing-review and editing, DS, GM, and RK; validation, GM, RS, and RK. All authors contributed to the article and approved the submitted version.

Funding

This work was partly supported by the Department of Electrical Engineering, Indian Institute of Technology Madras, Chennai, through the Science and Engineering Research Board (SERB) Teachers Associateship for Research Excellence Scheme, under Grant No. TAR/2020/000149.

Acknowledgments

The authors acknowledge and thank the DST-FIST funded Research laboratory of the Department of Electrical and Electronics Engineering, Kongu Engineering College, Perundurai - 638052, Erode, Tamil Nadu, India.

Conflict of interest

The authors declare that the research was conducted in the absence of any commercial or financial relationships that could be construed as a potential conflict of interest.

Publisher's note

All claims expressed in this article are solely those of the authors and do not necessarily represent those of their affiliated organizations, or those of the publisher, the editors and the reviewers. Any product that may be evaluated in this article, or claim that may be made by its manufacturer, is not guaranteed or endorsed by the publisher.

References

Amizhtan, S. K., Pawan Mahidhar, G. D., Sarathi, R., Taylor, N., and Edin, H. (2020). Investigation on electrical, thermal and mechanical properties of thermally aged pressboard impregnated with mixed mineral oil and synthetic ester fluid. *IET Sci. Meas. Technol.* 14 (10), 1029–1036. doi:10.1049/iet-smt.2020.0216

ASTM D3487-09 (2009). *Standard specification for mineral insulating oil used in electrical apparatus*. West Conshohocken, PA, USA: ASTM.

ASTM D6181-03 (2003). *Standard test method for measurement of turbidity in mineral insulating oil of petroleum origin (withdrawn 2012)*. West Conshohocken, PA, USA: ASTM.

ASTM D638-14 (2014). *Standard test method of tensile properties of plastics*. West Conshohocken, PA, USA: ASTM.

Carmela, O., Carrascal, I., Ferreño, D., Fernández, I., and Ortiz, A. (2021). Experimental dataset on the tensile and compressive mechanical properties of plain Kraft and crepe papers used as insulation in power transformers after ageing in mineral oil. *Data Brief* 36, 107031–107110. doi:10.1016/j.dib.2021.107031

Chinnasamy, V., Kumar Palaniappan, S., Anand Raj, M. K., Rajendran, M., and Cho, H. (2021). "Thermal energy storage and its applications," in *Materials for solar energy conversion: Materials. Methods and applications* (Hoboken, NJ,USA: wiley online library), 353–377.

CIE 109 - 1995 (1995). *A method of predicting corresponding colours under differentchromatic and illuminance adaptations, CIE 109 - 1995*. Vienna, Austria: CIE.

Coulibaly, M. L., Perrier, C., Marugan, M., and Beroual, A. (2013). Aging behavior of cellulosic materials in presence of mineral oil and ester liquids under various conditions. *IEEE Trans. Dielectr. Electr. Insulation* 20 (6), 1971–1976. doi:10.1109/tdei.2013.6678843

Dawei, F., Jian, H., Yang, L., Liao, R., Chen, X., and Li, J. (2020). Comparison of AC breakdown characteristics on insulation paper (pressboard) immersed by three-element mixed insulation oil and mineral oil. *High. Volt.* 5 (3), 298–305. doi:10.1049/hve.2019.0103

Dominic, J., Karthikeyan, M., and Satheesh Kumar, K. K. (2022). Polyaniline – rare Earth metal chloride composites as an adsorbent cum electrode material for supercapacitor performance investigation. *J. Energy Storage* 48 (103971), 103971–104010. doi:10.1016/j.est.2022.103971

IEC 60243-1 (2013). *Electric strength of insulating materials – test methods – Part 1: Tests at power frequencies*. Geneva, Switzerland: ICE Webstore.

IEC 60247 (2004). *Insulating liquids Measurement of relative permittivity, dielectric dissipation factor (tan) and d.c. resistivity*. Geneva, Switzerland: ICE Webstore.

IEC60156 (2003). *Third edition - insulating liquids–Determination of the breakdown voltage at power frequency–Test method*. Geneva, Switzerland: ICE Webstore.

Karthik, R., Raja Thangaswamy, S. R., and Sudhakar, T. (2013). Deterioration of solid insulation for thermal degradation of transformer oil. *Central Eur. J. Eng.* 3 (2), 226–232. doi:10.2478/s13531-012-0051-z

Lelekakis, N., Wijaya, J., Martin, D., and Susa, D. (2014). The effect of acid accumulation in power-transformer oil on the aging rate of paper insulation. *IEEE Electr. Insul. Mag.* 30 (3), 19–26. doi:10.1109/mei.2014.6804738

Liao, R. J., Tang, C., Yang, L. j., and Grzybowski, S. (2008). Thermal aging micro-scale analysis of power transformer pressboard. *IEEE Trans. Dielectr. Electr. Insulation* 15 (5), 1281–1287. doi:10.1109/tdei.2008.4656235

Neettiyath, A., Vasa, N. J., and Sarathi, R. (2021). Life expectancy estimation of thermally aged Cu contaminant-diffused oil impregnated pressboard. *IEEE Trans. Dielectr. Electr. Insulation* 28 (2), 637–645.doi:10.1109/tdei.2020.009197

Raj, R. A., and Murugesan, S. (2022). Optimization of dielectric properties of pongamia pinnata methyl ester for power transformers using response surface methodology. *IEEE Trans. Dielectr. Electr. Insulation* 29 (5), 1931–1939. doi:10.1109/tdei.2022.3190257

Raymon, A., and Karthik, R. (2015). Reclaiming aged transformer oil with activated bentonite and enhancing reclaimed and fresh transformer oils with antioxidants. *IEEE Trans. Dielectr. Electr. Insulation* 22 (1), 548–555. doi:10.1109/TDEI.2014.004094

Rontgen, B. G., and Mary Donnabelle, L. B. (2020). Adsorption of anionic methyl orange dye and lead(II) heavy metal ion by polyaniline-kapok fibre nanocomposite. *Mater. Chem. Phys.* 243 (122682), 1–8. doi:10.1016/j.matchemphys.2020.122682

Safiddine, L., Amel, H. Z., Fofona, I., Abdelhak, S., Fettouma, G., and Ahmed, B. (2017). Transformer oil reclamation by combining several strategies enhanced by the use of four adsorbents. *IET Generation, Transm. Distribution* 11 (11), 2912–2920. doi:10.1049/iet-gtd.2016.1995

Sangeetha, G., Viswapriya, R., Kaliyannan, R., Shanmugam, S., RajasekarGobinath, V., and Kumar Palaniappan, Sathish (2019). Wet corrosion behavior of copper exposed to recycled groundnut oil as biofuel. *Mater. Test.* 61 (2), 131–135. doi:10.3139/120.111294

Sarathkumar, D., Srinivasan, M., Palanichamy, M., and Antony Raj, R. (2022). Restoration of critical dielectric properties of waste/aged transformeroil using biodegradable biopolymer-activated clay compositefor power and distribution transformers. *Biomass Convers. Biorefinery* 12, 1–17. doi:10.1007/s13399-022-03065-0

Sathish Kumar, P., Rathanasamy, R., Chinnasamy, M.a, Pal, S. Kumar, and Kumar Jeganathan, S. (2023). "Green sustainable process for chemical and environmental engineering and science," in *Green solvent and extraction Technology* (Amsterdam, Netherlands: Elsevier), 1–16.

Segal, L., Creely, J. J., Martin, A. E., and Conard, C. M. (1959). An empirical method for estimating the degree of crystallinity of native cellulose using the X- ray diffractometer. *Text. Res. J.* 29 (10), 786–794. doi:10.1177/004051755902901003

Vasa, A. N. N. J., Vinu, R., and Sarathi, R. (2017). Influence of ambient medium on thermal ageing of pressboard in transformer oil containing dibenzyl bisulphide (DBDS). *IEEE Trans. Dielectr. Electr. Insulation* 24 (5), 2836–2846. doi:10.1109/tdei.2017.006412

Yashvi, S., Swapnil, D., Mohammad, K., and Shriram, S. (2021). An environment friendly approach for heavy metal removal from industrial wastewater using chitosan-based biosorbent: A review. *Sustain. Energy Technol. Assessments* 43 (100951), 109–143. doi:10.1016/j.seta.2020.100951

Yoshihara, H., and Yoshinobu, M. (2014). Off-axis tensile strength and evaluation of the in-plane shear strength of paper. *Holzforschung* 68 (5), 583–590. doi:10.1515/hf-2013-0163

Nomenclature

MO	Mineral Oil
RAMO	Recovered Aged Mineral Oil
FMO	Fresh Mineral Oil
AMO	Aged Mineral Oil
CTN-aB	Chitosan-activated Bentonite
PANI-c-KPF	Polyaniline coated Kapok Fibre
OIPB	oil-impregnated pressboard
PB	pressboard
XRD	X-ray diffraction
TGA	Thermogravimetric Analysis
DTG	Derivative Thermogravimetry
SEM	Scanning Electron Microscopy
FTIR	Fourier Transform Infrared
UV	Ultraviolet
IEC	International Electrotechnical Commission
ASTM	American Society for Testing and Materials
BV	Breakdown Voltage
CIE	International Commission on Illumination
DBP	2,6-di-tertiary-butyl-phenol
DBPC	2,6-di-tertiary-butyl-para-cresol